Atmos. Chem. Phys. Discuss., https://doi.org/10.5194/acp-2017-667
Manuscript under review for journal Atmos. Chem. Phys.
Discussion started: 28 August 2017

Atmospheric Chemistry and Physics Discussions

Concentrations and source regions of light absorbing impurities in snow/ice in northern Pakistan and their impact on snow albedo

Chaman Gul[1,2,5], Siva Praveen Puppala[2], Shichang Kang[1,3,5], Bhupesh Adhikary[2], Yulan Zhang[1], Shaukat Ali[4], Yang Li[3], Xiaofei Li[1]

[1]State Key Laboratory of Cryosphere Science, Northwest Institute of Eco-Environment and Resources, Chinese Academy of Sciences, Lanzhou 73000, China
[2]International Centre for Integrated Mountain Development (ICIMOD), G.P.O. Box 3226, Kathmandu, Nepal
[3]CAS Center for Excellence in Tibetan Plateau Earth Sciences, Beijing, 100101, China
[4]Global Change Impact Studies Centre (GCISC), Ministry of Climate Change, Islamabad, Pakistan
[5]University of Chinese Academy of Sciences, Beijing, China

Correspondence to: Chaman Gul (chaman.gul@icimod.org; chaman@lzb.ac.cn)

Abstract. Black carbon (BC), water-insoluble organic carbon (OC), and mineral dust are important particulate impurities in snow and ice, which significantly reduce albedo and accelerate melting. Surface snow and ice samples were collected from the Karakoram-Himalayan region of northern Pakistan during 2015 and 2016 in summer (six glaciers), autumn (two glaciers), and winter (six mountain valleys). The average BC concentration overall was 2130 ± 1560 ngg^{-1} in summer samples, 2883±3439 ngg^{-1} in autumn samples, and 992 ± 883 ngg^{-1} in winter samples. The average water insoluble OC concentration overall was 1839 ± 1108 ngg^{-1} in summer samples, 1423 ± 208 ngg^{-1} in autumn samples, and 1342 ± 672 ngg^{-1} in winter samples. The overall concentration of BC, OC, and dust in aged snow samples collected during the summer campaign was higher than the concentration in ice samples. The values are relatively high compared to reports by others for the Himalayas and Tibetan Plateau. This is probably the result of taking more representative samples at lower elevation where deposition is higher and the effects of ageing and enrichment more marked. A reduction in snow albedo of 0.1–8.3% for fresh snow and 0.9–32.5% for aged snow was calculated for selected solar zenith angles during day time using the Snow, Ice, and Aerosol Radiation (SNICAR) model. Daily mean albedo was reduced by 0.07–12.0%. The calculated radiative forcing ranged from 0.16 to 43.45 Wm^{-2} depending on snow type, solar zenith angle, and location. The potential source regions of the deposited pollutants were identified using spatial variance in wind vector maps, emission inventories coupled with backward air trajectories, and simple region tagged chemical transport modelling. Central, South, and West Asia were the major sources of pollutants during the sampling months, with only a small contribution from East Asia. Analysis based on the Weather Research and Forecasting (WRF-STEM) chemical transport model identified a significant contribution (more than 70%) from South Asia at selected sites. Research into the presence and effect of pollutants in the glaciated areas of Pakistan is economically significant because the surface water resources in the country mainly depend on the rivers (the Indus and its tributaries) that flow from this glaciated area.

Atmos. Chem. Phys. Discuss., https://doi.org/10.5194/acp-2017-667
Manuscript under review for journal Atmos. Chem. Phys.
Discussion started: 28 August 2017

Atmospheric Chemistry and Physics Discussions

1 Introduction

Carbon is an essential component of atmospheric aerosols, where it appears in the form of black carbon (BC, or elemental carbon EC), and organic carbon (OC). BC is emitted into the atmosphere from incomplete combustion of carbon-based fuels (mainly fossil fuels and biomass) (Jacobson, 2004) while OC can be directly emitted into or formed in the atmosphere. After deposition on snow and ice surfaces, BC particles significantly reduce the snow albedo (hemispheric reflectance) in the visible part of the electromagnetic spectrum, cause snow albedo feedback (Doherty et al., 2013), enhance solar radiation absorption (Warren and Wiscombe, 1980), and accelerate snow melting (Hansen and Nazarenko, 2004). BC, both in air and deposited on snow, is important in net positive forcing of the climate. Clean snow is one of the most reflective natural surfaces on Earth at the ultraviolet and visible wavelengths, while BC is the most efficient light-absorbing species in the visible spectral range (Horvarth, 1993). One ngg^{-1} of BC has almost the same effect on albedo reduction as 100 ngg^{-1} mineral dust at 500 nm wavelength (Warren et al., 1982). However, the exact amount of albedo reduction also depends on the refractive index, snow age, grain size, solar zenith angle (SZA), and dust particle size. Albedo reduction usually results in amplification of the energy absorbed by dirty snow (Painter et al., 2010). An albedo feedback is triggered and amplified by deposition of impurities on the snow surface which reduces snow albedo thus accelerating melting and further reducing albedo (Doherty et al., 2013; Flanner et al., 2009). Albedo feedback is amplified by the presence of light-absorbing impurities (Doherty et al., 2013). Studies conducted in Greenland showed that at visible wavelengths 10 ngg^{-1} coarse-grained BC particles in aged snow and 40 ngg^{-1} BC particles in new snow could reduce snow albedo by around 1 to 3% (Warren and Wiscombe, 1985).

Increased BC mass concentration and deposition on the Tibetan glaciers over the last 20 years (Xu et al., 2009a) has played a significant role in rapid glacier melting in the region (Xu et al., 2012; Yao et al., 2012). A high concentration of aerosol has deposited on the snow surface and increased the BC content in snow over the southern edge of the Tibetan Plateau to the north of the Himalayas (Gertler et al., 2016). The southern slope of the Himalayas is relatively even more exposed to BC due to emissions from India and transport through southwesterly and westerly winds (Xu et al., 2009; Yasunari et al., 2010). BC deposited on snow in the Himalayan region induces an increase in net shortwave radiation at the snow surface with an annual mean of about 1 to 3 Wm^{-2}, producing an estimated 0.05–0.3°C warming (Ménégoz et al., 2014). Deposition of anthropogenic BC has been observed to contribute significantly to the decrease in snow cover extent over recent decades (Dery et al., 2007), and shortening the duration of the snow cover season by several days (Ménégoz et al., 2013a). The climate warming efficiency of BC in snow is greater than the warming efficiency of other anthropogenic pollutants, including carbon dioxide (Hansen et al., 2005). The annual snow albedo reduction effect due to BC outweighs the aerosol dimming effect (reduction in solar radiation reaching the surface) by a factor of about six over the global snow cover (Flanner et al., 2009).

At present, South and East Asia are considered to be the two largest BC emission regions in the world and likely to remain so (Menon et al., 2010). BC transported from East Asia can be lifted high and moved towards the northeast during the summer monsoon season (Zhang et al., 2015; Cong et al., 2015; Lüthi et al., 2015), affecting the

life of glaciers and snow-covered areas.

Research into the glaciers of the extended Himalayan region and Tibetan Plateau has prime importance because these glaciers act as a water storage tower for South and East Asia, and shrinking could affect water resources for up to a billion people (Immerzeel et al., 2010). The glaciated area in northern Pakistan may be more exposed to BC effects than that in other regions because potentially it can receive emissions generated from both South and Central Asia as well as from the Middle East. Meltwater coming from these glaciers flows into the river Indus, which has major economic importance for the people of Pakistan.

A number of authors have described the concentration and impacts of light absorbing impurities in the Tibetan glaciers (for example Que et al., 2016; Zhang et al., 2017; Li et al., 2017; Niu et al., 2017;). However, until now, no studies have been published related to the concentration of light absorbing aerosols in the surface snow and ice of northern Pakistan, and although several authors have investigated transport pathways over the Himalayan region (e.g. Babu et al., 2011 for the western trans-Himalayas; Lu et al., 2012, and Kopacz et al., 2011 for the Tibetan Plateau and Himalayas) little is known about the potential sources and transport pathways of pollutants affecting the Pakistan area.

In this study, we looked at the concentration of light absorbing impurities (BC, OC, dust) in snow and ice in northern Pakistan, their impact on snow albedo and radiative forcing, and the likely source regions. Albedo was estimated from the BC and dust concentrations identified in collected samples of snow and ice using the online snow albedo simulation SNICAR model (Flanner et al., 2009). Radiative forcing was calculated from the albedo reduction obtained from the SNICAR model together with the incident short-wave solar radiation obtained from the SBDART (Santa Barbara DISORT Atmospheric Radiative Transfer) model. The frequency distribution of aerosol subtypes (smoke, continental polluted, dust, and others) in the atmosphere over the study area was calculated for the snow and ice sampling periods using CALIPSO satellite data from 2006 to 2014 as a further indication of the types of aerosol contributing to the observed deposition. The potential source regions of pollutants were identified using spatial variance in wind vector maps prepared using 50 years of reanalysis data, calculation of back air trajectories using the HYSPLIT-4 (Hybrid Single Particle Lagrangian Integrated Trajectory) model, and a simple region tagged chemical transport model (WRF-STEM). The back air trajectories approach has been used in many studies to identify possible source regions for atmospheric and deposited BC (Zhang et al., 2013). Pollutant source regions identified using the different approaches were compared and the most likely source regions of the pollutants identified.

2 Methodology

2.1 Study area

The study area was located around 35.40°N 74.38°E in the mountains and adjacent mountain valleys of the Karakoram and Himalayan region in northern Pakistan (Figure 1). Snow and ice samples were collected in summer from six glaciers – Passu, Gulkin, Barpu, Mear, Sachin, and Henarche – and in autumn from Gulkin and Sachin

(Figure 1). The Passu and Gulkin glaciers are located very near to the Karakoram highway connecting Pakistan with China, and there are a number of small villages (Passu, Hussaini, Gulmit, and others) close by. The Barpu and Mear glaciers are located very close to each other and around 2 km away from the residential area of the Hopar and Nagar valleys. There is a small city (Astore) near the Sachin glacier and some restaurants near its terminus. Winter snow samples were collected from mountain valleys near to Passu, Barpu and Sachin glaciers, and three other areas to the west with a number of small villages (Figure 1). The average elevation of the selected glaciers was quite low comparted to the elevation of the glaciers studied for BC, OC and dust on the Tibetan plateau by previous researchers. The mountains around the selected glaciers are mostly dry and rocky. The mean annual precipitation (rain) at Gilgit was approximately 0.412 ± 2 mm during the period 1980–2013 (Gul et al., 2017), while the daily average temperature during winter and pre-monsoon showed an increasing trend between 1980 and 2014 (Gul et al., 2017).The study area is mostly exposed to the westerlies and emission from South Asia. Most of the people in the region use wood for cooking and heating.

2.2 Sample collection

A total of 50 surface ice and 49 snow samples were collected from the glaciers in summer 2015 and 2016 (Passu 15, Gulkin 31, Barpu 6, Mear 8, Sachin 35, Henarche 4), and 13 in autumn 2016 (Gulkin 7, Sachin 6) at elevations ranging from 2,569 to 3,895 masl (Figure 1). Eighteen snow samples were collected in winter 2015 and 2016 from nearby mountain valleys at elevations of 1,958 to 2,698 masl; the winter sampling region was divided into six sites (S1 to S6) based on geographical location and elevation (Figure 1). Samples were collected using the "clean hands – dirty hands" principle (Fitzgerald, 1999). Ice samples were collected from the surface (5 cm depth) at different points on the glaciers. The elevation difference between collection points on the same glacier ranged from 30 to 100 meters.

The samples were preserved in ultra clean plastic bags, allowed to melt in a temporary laboratory near the sampling location, and filtered through quartz-filters immediately after melting. An electric vacuum pump was used to accelerate filtration. The melted snow/ice volume of the samples was measured using a graduated cylinder. Sampled filters were carefully packed inside petri-slides marked with a unique code representing the sample.

The snow density of winter snow samples was measured using a balance; snow/ice grain sizes were observed with a hand lens (25×) with an accuracy of 0.02 mm (Aoki et al., 2011).

2.3 Dust, OC, and BC analysis

Before analysis, sampled filters were allowed to dry in an oven for 24 hours and then weighed using a microbalance. The dust mass on the filters was calculated from the mass difference in weight before and after sampling (Kaspari et al., 2014; Li et al., 2017).

There are many methods available for analyzing BC and OC. The three methods considered most effective for measuring BC and water insoluble OC concentrations in snow are thermal optical analysis, filter-based analysis, and

single particle soot photometer analysis (Ming et al., 2008). The thermal optical analysis method has been used by many researchers (e.g., Li et al., 2017) and was chosen for the study. This is an indirect method for measuring BC and OC on sampled filters; it follows Beer's law and uses stepwise combustion of the impurities deposited on quartz filters (Boparai et al., 2008), followed by measurement of light transmission and/or reflectance of the filters. The BC and OC content present in the collected samples was measured using a thermal optical DRI carbon analyzer, similar to the IMPROVE protocol (Cao et al., 2003). A few (less than ten) filters had higher dust loads; for these the method was slightly modified using a 100% helium atmosphere and temperature plateau (550°C). A very few (less than 5) samples with very dense dust concentrations were not properly analyzed by the instrument and were excluded from the results. The extremely high dust value of one sample from Passu (15 times the level in the next highest sample) which had low values of other pollutants was excluded as a probable error. In some cases, a single sample was analyzed two or three times to ensure accurate results were obtained.

2.3.1 Frequency of different aerosol subtypes in the atmosphere

The frequency of different aerosol subtypes – clean marine, dust, polluted continental, clean continental, polluted dust, smoke, and other – present in the atmosphere over the study region was investigated using CALIPSO data for the same months in which ice and snow samples were collected i.e. January, May, June, and December – over the period June 2006 to December 2014. The Level 2 aerosol profile data products were downloaded from https://eosweb.larc.nasa.gov/project/calipso/aerosol_profile_table. A set of feature classification flags (including aerosol subtype) detected in different layers of the CALIPSO backscatter data were derived. The frequencies of different subtypes were calculated along the specific paths followed by CALIPSO over the study region.

2.4 Albedo simulations and estimation of radiative forcing

Light absorbing impurities (BC and dust particles) present on surface snow can reduce the snow surface albedo in the visible portion of the electromagnetic spectrum, increase solar radiation absorption, and accelerate melting (Yasunari et al., 2014). SZA, snow grain size, BC and dust concentration in snow, the presence of other light absorbing impurities, particle morphology, surface roughness, snow depth, liquid water content, snow shape, and topography are all important factors in reducing snow albedo (Wiscombe and Warren 1985).

Snow albedo was estimated for each of the 18 winter samples and the average calculated for samples at each of the sites (1 to 6). Albedo from two sites – S1 (Sost), which had the highest average concentration of BC and dust, and S6 (Kalam), which had the lowest average concentration of BC and dust – were further explored using the SNICAR model (Flanner et al., 2007). The aim was to quantify the effect of BC, dust, and Mass Absorption Cross section (MAC) on albedo reduction. Sensitivity model experiments were carried out using various combinations of BC, dust, and MAC values, while other parameters were kept constant (parameters for sites 1 and 6 shown in supplementary materials, Table S1). Snow albedo was simulated for different daylight times, with the SZA set in the range 57.0–88.9° based on the position of the sun in the sky for the sampling date and locations. The daily mean was

Atmos. Chem. Phys. Discuss., https://doi.org/10.5194/acp-2017-667
Manuscript under review for journal Atmos. Chem. Phys.
Discussion started: 28 August 2017

Atmospheric Chemistry and Physics Discussions

calculated from the mean of the albedo values simulated for 24 different SZA values (one per hour), and the daytime mean from the mean of the albedo values simulated for 10 SZA values (one per hour during daylight). The mid-latitude winter clear-sky option was selected for surface spectral distribution. The parameters used for sensitivity analysis are shown in Table S1. MAC values of 7.5, 11, and 15 m^2/g were selected based on a literature review (Que et al., 2014; Pandolfi et al., 2014). In order to reduce the uncertainty, the dust concentration in the samples was divided into four diameter classes (as per the model requirements): size 1 (0.1–1.0 µm) was taken to be 2%, size 2 (1–2.5 µm) to be 13%, size 3 (2.5–5 µm) to be 31%, and size 4 (5–10 µm) to be 54% of total dust mass present in the sample, based on results published by others (Gillette et al., 1974; Mahowald et al., 2014). Radiative forcing (RF) was estimated for the same samples following Eq. (1):

$$RF_x = R_{in-short} * \Delta \boldsymbol{\alpha}_x \quad (1)$$

where $R_{in\text{-}short}$ denotes incident short-wave solar radiation (daily mean), as measured by the SBDART (Santa Barbara DISORT Atmospheric Radiative Transfer) model, and $\Delta\alpha_x$ denotes the daily mean reduction in albedo, as simulated by the SNICAR model.

2.5 Source regions of pollutants

Black carbon particles have a residence time of days to weeks in the atmosphere (Cape et al., 2012) and may be transported a long way away from the source location (Kopacz et al., 2011; Aruna et al., 2013). Three methods were used to identify the potential source regions of pollutants found at the study site: wind maps, emissions inventory coupled with back trajectories, and a region-tagged chemical transport modeling analysis.

2.5.1 Wind maps

Wind speed and direction were represented using the two perpendicular vectors U (the zonal velocity towards the east) and V (the meridional velocity towards the north). Wind vector maps were prepared using 50 years of reanalysis data from the joint National Centers for Environmental Prediction and the National Center for Atmospheric Research (NCEP/NCAR) Reanalysis Project (available from the National Oceanic and Atmospheric Administration [NOAA] https://www.esrl.noaa.gov/psd/data/gridded/data.ncep.reanalysis.html). The U and V wind components were combined into a matrix around the study area for each individual month and then plotted against latitude/longitude values to show the spatial variance of monthly wind stress at 700 mb using arrows to indicate the direction and intensity of wind.

2.5.2 Back air trajectories

Air trajectories were calculated backwards from the sampling sites (S1: 36.40°N 74.50°E; S6: 35.46°N 72.54°E) to identify potential source regions for the pollutants using the web version of the Hybrid Single Particle Lagrangian Integrated Trajectory (HYSPLIT-4) model (Draxler and Hess, 1998). The HYSPLIT-4 model has been used by others to compute air mass trajectories to identify possible source regions (Ming et al., 2009; Zhang et al., 2013).

Reanalysis meteorological data from the same source as the wind data (https://www.esrl.noaa.gov/psd/data) were used as input data in the HYSPLIT model for May, June, and December 2015, and January 2016. HYSPLIT was run in a seven-day backward trajectory mode with trajectories initiating every six hours (0, 6, 12, and 18) on a daily basis from 4 May to 19 June 2015 and from 1 December 2015 to 31 January 2016. The HYSPLIT model results were combined with Representative Concentration Pathways (RCPs) emission data for 2010 (available from http://sedac.ipcc-data.org/ddc/ar5_scenario_process/RCPs.html) to identify the source location.

Monthly CALIPSO satellite based extinction data from 2006 to 2014 were used to calculate the vertical profile for aerosol extinction over the study region. The CALIPSO extinction profile was constructed for selected months – May and June for summer and December and January for winter – in 2006 to 2014 (Figure S1). The exponential equation $X = (\log(10.46) - \log(Y))/10.29$ was used to calculate the extinction profile for the trajectory heights, where Y is the vertical height in kilometers and X indicates the extinction against the height of trajectories. Height of individual trajectory points were put in the above equation and got a normalized extinction profile by assuming surface extinction =1(Figure S1).

2.5.3 WRF-STEM model

The WRF-STEM model was used as a third approach for identifying the origin (source regions) of air masses carrying pollutants. Region tagged CO tracer is a standard air quality modeling tool used by other regional and global chemical transport models to identify pollution source regions (Chen et al., 2009; Park et al., 2009; Lamarque and Hess, 2003). The WRF-STEM model uses region tagged carbon monoxide (CO) tracers for many regions in the world to identify geographical areas contributing to observed pollutants (Adhikary et al., 2010). The model domain centered on 50.377° E longitude and 29.917° N latitude. The model horizontal grid resolution was 45x45 km with 200 grids in the east-west direction and 125 north-south. The meteorological variables needed for the chemical transport were derived from the Weather Research and Forecast (WRF) meteorological model (Grell et al., 2005) using FNL data (ds083.2) available from the UCAR website as input data. The main aim of the simulation was to identify the geographic locations contributing to the observed pollutants at the field sites, thus emissions from open biomass burning were not included in the simulation. The simulations used the anthropogenic emissions from HTAPv2 (available from http://edgar.jrc.ec.europa.eu/htap_v2/), thus the results indicate the amount of pollutants reaching the study area from day-to-day planned and recurring activities in domestic, transport, industrial, and other sectors. The model was run for a month prior to the field campaign dates to allow for model spin up (normal practice for a regional chemical transport model), and then for the months of December, January, and June, to match the field campaign dates.

Atmos. Chem. Phys. Discuss., https://doi.org/10.5194/acp-2017-667
Manuscript under review for journal Atmos. Chem. Phys.
Discussion started: 28 August 2017

Atmospheric Chemistry and Physics Discussions

3. Results and discussion

3.1 BC, OC and dust concentrations

The minimum, maximum, and average concentrations of BC, OC, and dust in the ice and snow samples are given in Table 1. We represent water insoluble organic carbon as OC in this manuscript. The average BC concentration overall was 2130 ± 1560 ngg^{-1} in summer samples, 2883 ± 3439 ngg^{-1} in autumn samples (both from glaciers), and 992 ± 883 ngg^{-1} in winter samples. The average water insoluble OC concentration overall was 1839 ± 1108 ngg^{-1} in summer samples, 1423 ± 208 ngg^{-1} in autumn samples, and 1342 ± 672 ngg^{-1} in winter samples. There was considerable variation in individual samples, with summer values of BC ranging from 82 ngg^{-1} (Gulkin glacier) to 10,502 ngg^{-1} (Henarche glacier), autumn values from 125 ngg^{-1} (Gulkin glacier) to 6481 ngg^{-1} (Sachin glacier), and winter samples from 79 ngg^{-1} (Kalam) to 5957 ngg^{-1} (Sost).

The lowest BC (82 ngg^{-1}) and OC (128 ngg^{-1}) concentrations were observed in summer samples collected from the Gulkin and Sachin glaciers, respectively. The average values of BC and OC were low in all samples from the Passu glacier, even though it lies close to the Karakoram highway which links Pakistan with China. The low concentrations of BC may have been due to the east facing aspect of the glacier shielding it from pollutants transported from west to east. Slope aspect of a glacier is important for snow cover dynamics (Gul et al., 2017). Dust concentrations are known to vary with slope aspect due to the effects of wind direction on deposition.

The highest average concentration of BC was found in autumn samples from the Sachin glacier, and highest average concentration of OC in summer samples from the same glacier. The average concentration of BC was much greater in autumn than in summer on the Sachin glacier, but somewhat greater in summer than in autumn on the Gulkin glacier, indicating highly spatiotemporal patterns in the deposition of impurities. The marked difference on the Sachin glacier may have reflected the difference in the direction of air, which comes from Iran and Afghanistan in summer and the Bay of Bengal via India in autumn, with the generally lower deposition on the Gulkin glacier more affected by other factors.

Most summer samples were collected from surface ice (Figure S2a), but a few samples for Gulkin and Sachin were collected from aged snow on the glacier surface (Figure S2 b,c). Dust was visible on the relatively aged snow, and the BC and OC concentrations in these snow samples were much higher than those in ice. The highest average BC values in winter were also observed in aged snow (from Sost) and the lowest in fresh snow (from Kalam) (Table 1). Generally, snow samples collected within 24hours after snowfall event is considering as a fresh snow.

There was no clear correlation between average BC concentration of glacier samples and glacier elevation, while the winter snow samples showed a weak increasing trend in average BC with site elevation (Table 1, Figure S3).

We analyzed the ratios of OC to BC in the different samples as in atmospheric fractions this can be used as an indicator of the emission source, although apportionment is not simple and only indicative. The BC fraction is emitted during combustion of fossil fuels, especially biomass burning in rural areas in winter, and urban emissions from road transport. The OC fraction can be directly emitted to the atmosphere as particulate matter (primary OC) from fossil fuel emissions, biomass burning, or in the form of biological particles or plant debris; it can also be

Atmos. Chem. Phys. Discuss., https://doi.org/10.5194/acp-2017-667
Manuscript under review for journal Atmos. Chem. Phys.
Discussion started: 28 August 2017

generated in the atmosphere as gases are converted to particles (secondary OC). In general, lower OC/BC ratios are associated with fossil fuel emissions and higher OC/BC ratios with biomass burning. The lowest OC/BC ratio of 0.041 was observed in a summer sample from Henarche glacier, and the highest ratio of 5 in a winter sample from Kalam. The higher value at Kalam may indicate greater contributions from biomass burning than from fossil fuel combustion in the region. There was no clear correlation between BC and OC concentrations. In summer samples, the average concentration of OC was greater than the average concentration of BC in samples from four of the six glaciers, but it was much lower in Barpu and Henarche. In winter, individual snow samples indicated that concentration of OC was greater than BC at low elevation sites and vice versa; the average OC was greater than average BC at all except the highest elevation site (Table 1).

In deposited samples, low OC/BC ratios can result from a reduction in OC (Niu et al., 2017), greater contributions from BC enrichment and OC scavenging, and/or the contribution of different emission sectors (including quantity, combustion conditions, and fuel type). Often, the OC/BC ratio reflects the impact of dilution of dissolved organic carbon and enrichment of primary organic carbon during snow/ice melting, and differences in OC/BC ratios may reflect differences in the enrichment process. The low OC/BC ratio in the samples from Henarche, the glacier at the lowest elevation, could, for example, be due to preferential washing out of OC particles with meltwater. Overall, there was a higher positive correlation between BC and dust compared to OC suggesting that for BC and dust particle precipitation and enrichment processes were similar.

A wide range of values has been reported by different authors for BC concentrations in snow and ice samples from different regions (Table S2). The concentrations of BC in our samples were higher than those reported by many authors (Table S2), but were comparable with the results reported by Xu et al. (2012) in the Tien Shan Mountains, Li et al. (2016) in the northeast of the Tibetan plateau, and Wang et al. (2016) in northern China. High concentrations indicate high deposition rates on the snow and ice surface, but there are several possible reasons for a wide variation in values apart from differences in deposition rates, including differences in sampling protocols, geographical/sampling location (Qu et al., 2014) and elevation of sampling site, and year/season of sampling. The sampling season (May to September in our case) is an important factor because during the melting season rapid enrichment occurs immediately as snow melts. The peak melting period is May to August/September, thus the concentration of BC, OC, and dust in our samples would have been increased as melting progressed due to the enrichment in melting snow and scavenging by the melting water. In most cases snow and ice samples were collected quite a long time after snow fall, and the concentration of pollutants would also have increased in the surface snow and ice due to dry deposition. It seems likely that the pollutants in surface samples would be affected by sublimation and deposition until the next melt season (Yang et al., 2015). In some of the cases in our study, the average concentration of BC, OC, and/or dust for a particular glacier/site was increased as a result of a single highly concentrated sample, reflecting the wide variation that results from the interplay of many factors.

Enrichment is more marked at lower elevations as the temperatures are higher which enhances melting and ageing of surface snow, while deposition also tends to be higher because the pollutant concentrations in the air are

higher (Wang et al., 2012; Nair et al., 2013). Previous studies have tended to focus on the accumulation area of glaciers (e.g. ice cores and snow pits) where enrichment influences are less marked, and on high elevation areas, where deposition is expected to be lower, in both cases leading to lower values. In our study, the majority of samples collected in summer and autumn were collected from the ablation area of debris-covered glaciers where enrichment influences are marked due to the relatively high temperature, and this is reflected in the relatively high values of BC, OC, and dust. Li et al. (2017) showed a strong negative relationship between the elevation of glacier sampling locations and the concentration of light absorbing impurities. Stronger melt at lower elevations leads to higher pollutant concentrations in the exposed snow. Equally, BC may be enriched in the lower elevation areas of glaciers as a result of the proximity to source areas, as well as by the higher temperatures causing greater melting. Thus the main reason for the high concentrations of BC, OC, and dust in our samples may have been that the samples were taken from relatively low elevation sites. Human activities near the sampling sites in association with the summer pilgrimage season probably also contributed to an increase in pollutant concentrations.

3.2 Frequency distribution of aerosol sub types in the atmosphere

The frequency of different aerosol subtypes present in the atmosphere over the study region was investigated using CALIPSO subtype aerosol data (clean marine, dust, polluted continental, clean continental, polluted dust, smoke, and other) for January, May, June, and December (the months in which samples were collected) from June 2006 to December 2014. The frequency was calculated along the tracks followed by the CALIPSO satellite. Frequency for the month of June in 2006 to 2014 is shown in Figure S4. Figure 2 shows the seasonal results for month of May, June (summer) and December, January (winter) in the form of a box plot. During Jun smoke had the highest frequency (39%), followed by dust (21%), polluted dust (12%), and others (20%) Figure S4. Overall Smoke, dust and or polluted dust were the dominant subtype aerosols in selected months over the study region. Pollutant deposition depends on the concentration of pollutants in the atmosphere, the results are consistent with the high concentration of BC (from smoke) and dust particles in the glacier and snow surface samples

3.3 Snow albedo reduction

The albedo of individual winter snow samples was calculated using the SNICAR model and then averaged for each site (S1 to S6). Figure 3a shows the average for each site across the visible and infrared spectrum. Two sites were chosen for further analysis: S1 (Sost) which had the highest average concentration of BC, and S6 (Kalam) which had the lowest average concentration of BC. The albedo was simulated for different MAC values and SZA for samples at the two sites as described in the methods. The values for average albedo of samples from the two sites simulated at a wavelength of 0.975 μm for MAC values of 7.5, 11, and 15 m^2/g and SZA of 57.0–88.9° (day time) under a clear sky ranged from 0.39 (site S1, BC only, midday, MAC 15 m^2/g) to 0.85 (site S6, dust only, early evening, MAC 7.5–15 m^2/g). The detailed values are shown in Table S3.

Table 2 show the calculated percentage reduction (compared to a reference value with zero BC, OC, and dust) in

daily minimum, maximum, and mean broadband snow albedo at different MAC values (7.5, 11, 15 m^2/g) resulting from the average BC, dust, and combined BC and dust concentrations found in samples at each of the sites. The reduction was strongly dependent on BC concentration and almost independent of dust concentration, and increased with increasing MAC value. The results suggest that BC was the dominant forcing factor, rather than dust, as a result of the rapid snowmelt. BC was found to play an important role in forcing in the northern Tibetan plateau (Li et al., 2016), whereas in the central Tibetan plateau and Himalayas, dust played a more important role (Qu et al., 2014; Kaspari et al., 2014). The MAC value affected the albedo more in the visible range than at 1.2 μm (near infrared) wavelength (Fig 3c,d). The combined concentration of BC and dust, or BC alone, strongly reduced the snow albedo for a given combination of other input parameters. The effect at the low pollutant site (S6) was small: the values for day time snow albedo at 0.975 μm due to BC, or BC plus dust with different MAC and SZA, ranged from 0.70 to 0.83, with a reduction in daily mean albedo of 1.8 to 2.9%, and those for dust alone from 0.79 to 0.85, with a reduction in daily mean albedo of less than 0.1%. The effect at the high pollutant site (S1) was much more marked: BC or BC and dust reduced day time snow albedo to values ranging from 0.39 to 0.64, a reduction in daily mean albedo of 8.8 to 12.0%, but the effect of dust alone was still low with values of 0.70 to 0.78, again a reduction in daily mean albedo of less than 0.1%.

Both the snow albedo and the impact of impurities depend on a range of factors including the SZA, snow depth, snow grain size, and snow age. For example, the snow albedo reduction due to BC is known to be less in the presence of other light absorbing impurities as these will absorb some of the available solar radiation (Kaspari et al., 2011). The snow albedo calculated for our samples was strongly dependent on the SZA with albedo increasing with decreasing SZA, especially at near infrared wavelengths (Table S3).

The impact of snow ageing was also investigated. The winter samples from S1 (Sost) were aged snow, whereas those from S6 (Kalam) were fresh snow (Table 1, Figure S5 b,c). Not only was dust clearly visible on the surface of the aged snow, the grain size was large and the snow was dense. The aged snow had a much higher concentration of BC and dust, which reduced the albedo, but the extent of reduction is also affected by other factors. Albedo reduction by BC and dust particles is known to be greater for aged snow than for fresh snow (Warren and Wiscombe, 1985). In our samples, the calculated reduction in snow albedo for high MAC values (15) compared to low MAC values (7.5) was greater in aged snow than in fresh snow (Figure 3b). The effective grain size of snow increases with time as water surrounds the grains. Snow with larger grain size absorbs more radiation because the light can penetrate deeper into the snowpack, thus decreasing surface albedo (Flanner et al., 2006). In the melting season, the snowpack becomes optically thin and more impurities are concentrated near the surface layer, which further increases the effect on albedo.

The estimated reduction in snow albedo by dust and BC compounded by the age of snow (up to 29% of daytime maximum value, Table 2) was higher than that reported by others for High Asia based on farmers' recordings (e.g 1.5 to 4.6% reported by Nair et al., 2013) and in the Himalayas (Ming et al., 2008; Kaspari et al., 2014; Gertler et al., 2016). However, although the values were relatively high, they were at the same level or lower than the estimates for

albedo reduction of 28% by BC and 56% by dust in clean ice samples, and of 36% by BC and 29% by dust in aged snow samples, reported by Qu et al. (2014) for surface samples from the Zhadang glacier, China. Simulation results by Ming et al. (2013a) showed BC, dust, and grain growth to reduce broadband albedo by 11%, 28%, and 61%, respectively, in a snowpack in central Tibet. Dust was the most significant contributor to albedo reduction when mixed inside the snow and ice, or when the glacier was covered in bare ice. In our case BC was a more influential factor than dust during a similar study period to that reported by Li et al. (2017), indicating that BC plays a major role in albedo reduction.

The possible reasons for the relatively high values for albedo reduction in our samples include the lower elevation of the sampling locations, relatively high concentrations of BC and dust, high MAC values, low snow thickness, underlying ground quality, presence of small and large towns near the sampling sites, and predominance of aged snow samples. Most of the samples collected in winter were from places with snow depth less than 50 cm (Figure S5a), thus mud, stones, and clay below the snow layer would be expected to increase the absorption of solar radiation and reduce the albedo.

The high albedo reduction in the visible range of the electromagnetic spectrum could be due to the relatively high concentration of surface (~1cm) snow impurities. The total amount of deposited impurities in the surface layer of aged snow was relatively high, indicating a high deposition rate of atmospheric pollutants.

Flanner et al. (2007) reported that BC emission and snow ageing are the two largest sources of uncertainty in albedo estimates. The uncertainties in our estimated albedo reduction include the BC type (uncoated or sulfate coated), exact snow age, the size distribution of dust concentration, the accuracy of snow grain size, snow density, and albedo of the underlying ground. Sulfate-coated particles have an absorbing sulfate shell surrounding the carbon; recent studies confirm that coated BC has a larger absorbing power than non-coated BC (Naoe et al., 2009). We used uncoated black carbon concentration in the SNICAR model, but the pollutants at the remote site are presumed to be mainly from long range transport, thus the BC may have gained some coating. The albedo reduction for sulfate-coated black carbon was calculated to be 3–8.5% higher, depending on the MAC and SZA values, than for uncoated black carbon at low concentrated site S6 (Figure S6).

3.4 Radiative forcing (RF)

Radiative forcing (RF) is a measure of the capacity of a forcing agent to affect the energy balance in the atmosphere – the difference between sunlight absorbed by the Earth and energy radiated back to space – thereby contributing to climate change. Changes in albedo contribute directly to radiative forcing: a decrease in albedo means that more radiation will be absorbed and the temperature will rise. In snow and ice, the additional energy absorbed by any pollutants present also increases and accelerates the melting rate.

Various authors have described the impact of albedo change in snow and ice on radiative forcing. Zhang et al. (2017) reported that a reduction in albedo by 9% to 64% can increase the instantaneous radiative forcing by as much as 24.05–323.18 Wm^{-2}. Nair et al. (2013) estimated that in aged snow a BC concentration of 10–200 ngg^{-1} can

increase radiative forcing by 2.6 to 28.1 Wm^{-2}; while Yang et al. (2015) reported radiative forcing of 18–21 Wm^{-2} for aged snow in samples from the westernmost Tibetan Plateau.

We calculated the radiative forcing in the samples assessed for day time albedo and daily (24h) mean albedo. The radiative forcing at different daylight times caused by BC deposition varied from 3.93 to 43.44 Wm^{-2} (3.93–11.54 Wm^{-2} at the low BC site and 20.88–43.45 Wm^{-2} at the high BC site), and that by dust from 0.16 to 2.08 Wm^{-2} (0.16–0.30 Wm^{-2} at the low BC site and 1.38–2.08 Wm^{-2} at the high BC site) (detailed values given in Table S4), indicating that BC was the dominant factor. The RF due to combined BC and dust was very similar to that for BC alone. The increase in daily mean radiative forcing ranged from 0.1% for dust only at the low pollutant site to 14.9% for BC at the high pollutant site.

Both radiative forcing and albedo reduction increased with decreasing daytime SZA, indicating higher melting at midday compared to morning and evening. Figure 4 shows the daily mean albedo reduction and corresponding radiative forcing caused by BC for fresh (low BC) and aged (high BC) snow with different MAC values. An increase in MAC value from 7.5 to 15 led to an increase in radiative forcing by 1.48 Wm^{-2} in fresh snow and 4.04 Wm^{-2} in aged snow. This suggests that when the surface of snow, ice, and glaciers experience strong melting, enrichment with BC and dust could cause more forcing. Previous studies of ice cores and snow pits probably underestimated the albedo reduction and radiative forcing in glacier regions as samples were taken from high elevation areas where there is less ageing and melting and thus lower surface enrichment of BC and dust than at lower elevation. Our results are higher than those reported in other studies on the northern slope of the Himalayas (Ming et al., 2012), western Tibetan Plateau (Yang et al., 2015b), and Tien Shan mountains (Ming et al., 2016). However, they are comparable to values for radiative forcing reported more recently by others, for example for the Muji glacier (Yang et al., 2015), Zhadang glacier (Qu et al., 2014), in high Asia (Flanner et al., 2007; Nair et al., 2013), and in the Arctic (Wang et al., 2011; Flanner, 2013). The results suggest that enrichment of black carbon (in our case) and mineral dust (other authors) can lead to increased absorption of solar radiation, exerting a stronger effect on climate and accelerating glacier melt.

3.5 Potential source regions

3.5.1 Wind vector maps

Figure 5 shows the spatial variance of wind vector maps (U and V) at 700 mb in May, June, January, and December prepared using 50 years of reanalysis data. The wind blows primarily from west to east but there were variations over the year. Central and South Asia contributed a large part of the air in December, January, and May. In winter (December and January), the wind blew from Azerbaijan and northwest Iran, reaching the study site via Syria, Iraq, Turkmenistan, and Afghanistan. In May, the prevailing air masses were from Syria, Turkey, Turkmenistan, Iraq, Azerbaijan, northwest Iran, Afghanistan, and southern Pakistan. In June, the trend shifted gradually towards air arriving from the east (Myanmar and Thailand) through the Bay of Bengal, India, the Arabian Sea, and southeast Pakistan, especially to lower elevation areas, becoming dominated by these easterlies in autumn.

436 In November and December, the western trade winds again became stronger than the easterlies.

437 **3.5.2 Coupled emissions inventory with back air trajectory**

438 Trajectory analysis using the HYSPLIT model showed that in May and June 2015 air parcels reached the study
439 site along three different pathways: one from north Asia (Russia) via Central Asia (Kazakhstan), one from western
440 Asia (Cyprus and Syria) via Central and Southern Asia (Georgia), and one via India, which was more local (Figure
441 6). The trajectories in summer had distinct pathways, while those in winter were dispersed in all directions, partially
442 covering West, East, and South Asia, and completely covering Central Asia. Figure 6 shows the product of
443 extinction and emission calculated along the pathways of trajectories calculated using the vertical profile for aerosol
444 extinction over the study region obtained from the monthly CALIPSO satellite-based extinction data. Scattering and
445 absorption decreased exponentially with increasing elevation (Figure S1) but was still visible at elevations above 5
446 km in summer.
447 The RCP emission data combined with back trajectories and extinction data showed that the hotspot regions of
448 pollution that affected the study sites during winter were mainly to the southwest rather than very distant (Figure
449 6b). Iran, Turkmenistan, Azerbaijan, Georgia, the eastern part of Turkey, and the southwestern part of Russia all
450 showed comparatively high pollutant emissions in winter which moved towards northern Pakistan. The western part
451 of Kazakhstan, Uzbekistan, and northeastern Turkey emitted particularly high concentrations of pollutants.
452 Combination of the back-trajectory results and surface-wind direction analysis indicated that during the sampling
453 months, aerosols were significantly influenced by the long-range transport of pollutants coming from Central and
454 South Asia, with a small contribution from West and East Asia. This differs somewhat from previous reports which
455 suggested that the Tibetan Plateau and Himalayan region are mainly effected by pollutants from East and South Asia
456 (Zhang et al., 2015). An increasing trend has been reported for black carbon emissions in Central and South Asia
457 over the past 150 years (Bond et al., 2007), and a significant increase has been found in black carbon concentrations
458 in glacier snow in west China in the last 20 years, especially during the summer and monsoon seasons (Ming et al.,
459 2008). In South Asia, the largest source of atmospheric black carbon is emission from biomass and biofuels used for
460 cooking and heating (dung, crop residues, wood) (Venkataraman et al., 2005).
461 BC from East Asia can potentially be lifted up high and transported to the northeast during the summer monsoon
462 season (Zhang et al., 2015). Nevertheless, the results indicate that only a low level of pollutants reached the study
463 area from this source. BC particles emitted from distant low latitude source regions such as South Africa barely
464 reach the Tibetan Plateau and Himalayan regions because their weak emissions are removed along the transport
465 pathways during the summer monsoon season (Zhang et al., 2015).

466 **3.5.3 Chemical transport modelling**

467 The contribution of pollutants from potential source regions was also investigated using the WRF-STEM model
468 with tagged carbon monoxide tracers and source regions of East Asia, South Asia, Central Asia, the Middle East,

Europe, the Russian Federation, and West Asia. (The individual countries in the regions are listed in Table S5).

Figure 7 shows the results of the model simulations for summer (1 June to 4 July 2015) and winter (15 December 2015 to 17 January 2016) at two glacier sites (Sachin and Shangla) where the model terrain elevation was close to the observation terrain elevation. The model simulations showed Pakistan to be the major contributor of pollutants in summer (77% at Shangla and 43% at Sachin) followed by the South Asian countries; and the south Asian countries in winter (47% at Shangla and 71% at Sachin) followed by Pakistan, which is in line with the findings by Lu et al. (2012) that South Asia contributed 67% black carbon in the Himalayas. There were minor contributions of 2–7% of pollutants from Afghanistan, Iran, Central Asia, and the Middle East, and extremely small amounts from East Asia, Europe, Africa, West Asia, and China. The contribution from Iran, the Middle East, and Europe was greater in winter than in summer, while the contribution from Central Asia and China was greater in summer than in winter. The proportion of daily contributions fluctuated considerable: with higher contributions from Iran, the Middle East, and Europe on individual days in winter, ranging for example from 2–30% for the Middle East.

The concentration of hydrophobic BC (BC1), hydrophilic BC (BC2), and total black carbon (BC = BC1 + BC2) given by the model for Sachin glacier grid point in the summer and winter seasons is shown in supplemental material (Figure S7). Freshly emitted BC particles are hydrophobic and gradually acquire a hygroscopic coating over time in the model. Time series analysis of BC1 and BC2 concentration show influence of both freshly emitted BC as well as aged BC reaching the observation location. The highest concentration of BC1 was observed on 20th December 2015 followed by 25th June 2015, indicating influence of freshly emitted air mass both in the summer as well as winter months. Future study will evaluate the details of the different source region of BC reaching the glaciers as compared to region tagged CO tracers.

3.5.4 Comparison of the different approaches used to identify potential source regions

The high BC concentration in the atmosphere over the study region was attributed to long-range transport from urban source regions. Potential source regions of the pollutants deposited on glaciers and snow were identified using wind vector mapping with 50 years of reanalyzed data, calculation of back air trajectories using the HYSPLIT-4 model, and chemical transport pathways using the WRF-STEM tagged chemical transport model. The back trajectory results indicated that the majority of pollutants in summer were from Central and South Asia, and in winter from Iran, Pakistan, Iraq, Turkmenistan, Azerbaijan, Georgia, Jordan, Syria, Tunisia, Ukraine, Libya and Egypt. The WRF-STEM model indicated that most anthropogenic pollutants were from Pakistan and South Asia during both summer and winter. However, both approaches showed a reasonable contribution from Central Asian countries and limited contribution from East Asian countries in summer. The wind vector maps also indicated that the study site was mostly effected by westerly winds. All three approaches showed a reasonable contribution from neighboring countries such as Afghanistan, Pakistan, Iran, and India in specific months. Overall, the results indicate that South, Central, and West Asia were the major sources of the pollutants detected at the sampling sites.

There was some mismatching in source regions among the three approaches. The WRF-STEM model and wind vector maps both identified a small contribution from East Asia, but this was not identified in the back trajectories approach. Similarly, the wind vector maps and back air trajectories showed a dominant contribution from the west, while the WRF-STEM model showed a major contribution from Pakistan and South Asia. The differences in the results obtained by the different methods may be due in part to the complex topography of the region and the different altitudes used by the methods; the coarse resolution of the WRF-STEM model; and differences in the emission source inventories and meteorological parameters used by the WRF-STEM and HYSPLIT-4 models. Limitation of using back trajectories to identify source region is explained further in a paper by (Jaffe et al., 1999).

Furthermore, the atmospheric BC concentration over the Himalayas has significant temporal variations associated with synoptic and meso scale changes in the advection pattern (Babu et al., 2011) which can affect pollutant transport and deposition. The large uncertainty among different emission inventories can also affect the results, especially in the Himalayan region.

4 Summary and conclusion

Black carbon (BC) and organic carbon (OC) concentrations were measured using thermal optical analysis of snow and ice surface samples collected from glacier and mountain valleys in northern Pakistan in summer, autumn, and winter. The samples contained high concentrations of BC, OC, and dust. The samples from Sost contained the highest average concentration of BC in mountain valleys snow (winter) and those from Kalam the lowest, probably due to the impact of snow age (the Sost samples were aged snow and Kalam samples fresh snow), and increased grain size and density. The average concentration of BC in surface samples from Sachin glacier was higher in autumn than in summer; the BC values in summer snow samples collected from Sachin and Gulkin glaciers (aged snow from the glacier surface) were much higher than those in ice. The average BC concentration in summer samples collected from glaciers was 2130 ± 1560 ngg^{-1} and that in autumn samples 2883± 3439ngg^{-1}. The average concentration of OC was 1839 ± 1108 ngg^{-1} in summer samples, 1423 ± 208 ngg^{-1} in autumn samples, and 1342 ± 672 ngg^{-1} in winter samples, with the highest variability in summer samples. The individual lowest BC (82 ngg^{-1}) and OC (129 ngg^{-1}) concentrations were observed in summer samples collected from the Gulkin and Sachin glaciers, respectively. Dust and other pollutants were clearly visible on aged snow and ice surfaces; the results indicate considerable enrichment during ageing. The pollutant concentrations in our samples were relatively higher than those reported by others in earlier studies, which tended to focus on the accumulation area of glaciers (e.g. ice cores and snow pits), where enrichment influences are less marked and measured values are likely to be lower, and high elevation areas, where deposition of pollutants is expected to be lower. It is likely that pollutant concentrations were underestimated in these earlier studies, particularly when there was strong surface melting.

Snow albedo was calculated for winter samples using the SNICAR model with various combinations of BC and dust concentrations, three values for MAC, and a range of values for SZA (57 – 88.89º during daytime), with other parameters kept constant. BC was the major component responsible for albedo reduction, dust had little effect. The

reduction by BC ranged from 2.8 to 32.5% during daytime, which is quite high, with albedo reduced to below 0.6. The reduction was greater for higher concentrations of BC and greater MAC. The reduction in 24 h average albedo ranged from <0.07–2.9% for fresh snow samples and <0.05–12.0% for aged snow. Changes in albedo contribute directly to radiative forcing: a decrease in albedo means that more radiation will be absorbed and the temperature will rise. The radiative forcing by BC was also higher than that caused by dust, indicating that BC was the dominant factor. The day time albedo values in winter snow samples ranged from 0.39 to 0.82 with BC alone or BC plus dust, and from 0.70 to 0.85 with dust alone; the corresponding radiative forcing was 3.93–43.44 Wm^{-2} for BC alone, 4.01–43.45 Wm^{-2} for BC and dust, and 0.16–2.08 Wm^{-2} with dust alone. The radiative forcing calculated from the daily mean albedo reduction ranged from 0.1% for dust only at the low pollutant site to 14.9% for BC at the high pollutant site.

The potential source regions of the pollutants deposited on glaciers and snow were identified using spatial variance in wind vector maps, emission inventories coupled with back air trajectories, and region tagged chemical transport modelling. The wind vector maps identified Central Asian and South Asian countries (such as Azerbaijan, Turkmenistan, Pakistan, Afghanistan, Syria, Iraq, Turkey) as more important. The trajectory analysis coupled with emission inventories showed that air parcels reached northern Pakistan along three pathways, one from north Asia (Russia) via Central Asia (Kazakhstan), one from western Asia (Cyprus and Syria) via Central and Southern Asia (Georgia), and one via India. Combination of the back-trajectory results and surface-wind direction analysis indicated that aerosols were significantly influenced by the long-range transport of pollutants from Central and South Asia. The region tagged chemical transport model indicated that Pakistan and South Asia were the main contributors of pollutants. Analysis based on the WRF-STEM model identified a significant contribution from Pakistan (up to 77%) and South Asia (up to 71%) at selected sites. Overall, the results indicate that Central, South, and West Asia were the major sources of the pollutants detected at the sampling sites, with only a small contribution from East Asia.

Acknowledgments

This study was supported by the National Natural Science Foundation of China (41630754, 41671067, and 41501063), the Chinese Academy of Sciences (KJZD-EW-G03-04), the State Key Laboratory of Cryosphere Science (SKLCS-ZZ-2015), program funding to ICIMOD from the Governments of Sweden and Norway, and ICIMOD core funds contributed by the Governments of Afghanistan, Australia, Austria, Bangladesh, Bhutan, China, India, Myanmar, Nepal, Norway, Pakistan, Switzerland, and the United Kingdom. The authors wish to thank the unknown reviewers for their invaluable comments and advice on an earlier draft.

References

Adhikary, B., Carmichael, G. R., Kulkarni, S., Wei, C., Tang, Y., D'Allura, a., Mena-Carrasco, M., Streets, D. G.,

Zhang, Q., Pierce, R. B., Al-Saadi, J. a., Emmons, L. K., Pfister, G. G., Avery, M. a., Barrick, J. D., Blake, D. R., Brune, W. H., Cohen, R. C., Dibb, J. E., Fried, a., Heikes, B. G., Huey, L. G., O'Sullivan, D. W., Sachse, G. W., Shetter, R. E., Singh, H. B., Campos, T. L., Cantrell, C. a., Flocke, F. M., Dunlea, E. J., Jimenez, J. L., Weinheimer, a. J., Crounse, J. D., Wennberg, P. O., Schauer, J. J., Stone, E. a., Jaffe, D. a. and Reidmiller, D. R.: A regional scale modeling analysis of aerosol and trace gas distributions over the eastern Pacific during the INTEX-B field campaign, Atmos. Chem. Phys., 10(5), 2091–2115, doi:10.5194/acp-10-2091-2010, 2010.

Aoki, T., Kuchiki, K., Niwano, M., Kodama, Y., Hosaka, M. and Tanaka, T.: Physically based snow albedo model for calculating broadband albedos and the solar heating profile in snowpack for general circulation models, J. Geophys. Res. Atmos., 116(11), 1–22, doi:10.1029/2010JD015507, 2011.

Aruna, K., Kumar, T. V. L., Rao, D. N., Murthy, B. V. K., Babu, S. S. and Moorthy, K. K.: Black carbon aerosols in a tropical semi-urban coastal environment: Effects of boundary layer dynamics and long range transport, J. Atmos. Solar-Terrestrial Phys., 104(March), 116–125, doi:10.1016/j.jastp.2013.08.020, 2013.

Babu, S. S., Chaubey, J. P., Krishna Moorthy, K., Gogoi, M. M., Kompalli, S. K., Sreekanth, V., Bagare, S. P., Bhatt, B. C., Gaur, V. K., Prabhu, T. P. and Singh, N. S.: High altitude (~4520 m amsl) measurements of black carbon aerosols over western trans-Himalayas: Seasonal heterogeneity and source apportionment, J. Geophys. Res. Atmos., 116(24), 1–15, doi:10.1029/2011JD016722, 2011.

Bond, T. C., Bhardwaj, E., Dong, R., Jogani, R., Jung, S., Roden, C., Streets, D. G. and Trautmann, N. M.: Historical emissions of black and organic carbon aerosol from energy-related combustion, 1850-2000, Global Biogeochem. Cycles, 21(2), 1–16, doi:10.1029/2006GB002840, 2007.

Boparai, P., Lee, J. and Bond, T. C.: Revisiting Thermal-Optical Analyses of Carbonaceous Aerosol Using a Physical Model, Aerosol Sci. Technol., 42(11), 930–948, doi:10.1080/02786820802360690, 2008.

Cao, J. J., Lee, S. C., Ho, K. F., Zhang, X. Y., Zou, S. C., Fung, K., Chow, J. C. and Watson, J. G.: Characteristics of carbonaceous aerosol in Pearl River Delta Region, China during 2001 winter period, Atmos. Environ., 37(11), 1451–1460, doi:10.1016/S1352-2310(02)01002-6, 2003.

Cape J. N., Coyle. M., Dumitrean, P.: The atmospheric lifetime of black carbon, J. Atmospheric Environment, Volume 59, doi.org/10.1016/j.atmosenv.2012.05.030, 2012.

Chen, D., Wang, Y., Mcelroy, M. B., He, K., Yantosca, R. M. and Sager, P. Le: and Physics Regional CO pollution and export in China simulated by the high-resolution nested-grid GEOS-Chem model, , (2008), 3825–3839, 2009.

Cong, Z., Kawamura, K., Kang, S., Fu, P., River, G., River, Y. and River, Y.: Penetration of biomass-burning emissions from South Asia through the Himalayas : new insights from, , 1–7, doi:10.1038/srep09580, 2015.

Déry, S. J. and Brown, R. D.: Recent Northern Hemisphere snow cover extent trends and implications for the snow-albedo feedback, Geophys. Res. Lett., 34(22), 2–7, doi:10.1029/2007GL031474, 2007.

Doherty, S. J., Grenfell, T. C., Forsström, S., Hegg, D. L., Brandt, R. E. and Warren, S. G.: Observed vertical redistribution of black carbon and other insoluble light-absorbing particles in melting snow, J. Geophys. Res.

Atmos., 118(11), 5553–5569, doi:10.1002/jgrd.50235, 2013.

Draxler, R. R. and Hess, G. D.: An Overview of the HYSPLIT_4 Modelling System for Trajectories, Dispersion, and Deposition, Aust. Meteorol. Mag., 47(February), 295–308, 1998.

Fitzgerald, W. F.: Clean hands, dirty hands: Clair Patterson and the aquatic biogeochemistry of mercury, Clean Hands, Clair Patterson's Crusade Against Environmental Lead Contamination, 119–137, 1999.

Flanner, M. G.: Arctic climate sensitivity to local black carbon, J. Geophys. Res. Atmos., 118(4), 1840–1851, doi:10.1002/jgrd.50176, 2013.

Flanner, M. G. and Zender, C. S.: Linking snowpack microphysics and albedo evolution, J. Geophys. Res. Atmos., 111(12), 1–12, doi:10.1029/2005JD006834, 2006.

Flanner, M. G., Zender, C. S., Randerson, J. T. and Rasch, P. J.: Present-day climate forcing and response from black carbon in snow, J. Geophys. Res. Atmos., 112(11), 1–17, doi:10.1029/2006JD008003, 2007.

Flanner, M. G., Zender, C. S., Hess, P. G., Mahowald, N. M., Painter, T. H., Ramanathan, V. and Rasch, P. J.: Springtime warming and reduced snow cover from carbonaceous particles, Atmos. Chem. Phys. Discuss., 8(6), 19819–19859, doi:10.5194/acpd-8-19819-2008, 2009.

Gertler, C. G., Puppala, S. P., Panday, A., Stumm, D. and Shea, J.: Black carbon and the Himalayan cryosphere: A review, Atmos. Environ., 125(SEPTEMBER), 404–417, doi:10.1016/j.atmosenv.2015.08.078, 2016.

Gillette, D.A., Blifford, I.H., Fryrear, D.W.: Influence of wind velocity on size distributions of aerosols generated by wind erosion of soils. J. Geophys. Res. 79, 4068–4075, doi: 10.1029/JC079i027p04068, 1974.

Grell, G. A., Peckham, S. E., Schmitz, R., McKeen, S. A., Frost, G., Skamarock, W. C. and Eder, B.: Fully coupled chemistry within the WRF model, Atmos. Environ., 39(37), 6957–6975, doi:DOI: 10.1016/j.atmosenv.2005.04.027, 2005.

Gul, C., Kang, S. et al.: Using Landsat images to monitor changes in the snow-covered area of selected glaciers in northern Pakistan, Journal of Mountain Science, DOI：10.1007/s11629-016-4097-x.2017.

Hansen, J. and Nazarenko, L.: Soot climate forcing via snow and ice albedos, Proc. Natl. Acad. Sci. U. S. A., 101(2), 423–428, doi:10.1073/pnas.2237157100, 2004.

Hansen, J., Sato, M., Ruedy, R., Nazarenko, L., Lacis, A., Schmidt, G. A., Bell, N.:Climate and Dynamics-D18104-Efficacy of climate forcings, J. Geophys. Res., Part D-Atmospheres, 110(18), doi: 10. 1029/2005JD005776, 2005.

Immerzeel, W. W., van Beek, L. P. H. and Bierkens, M. F. P.: Climate change will affect the Asian water towers., Science, 328(5984), 1382–5, doi:10.1126/science.1183188, 2010.

Jacobson, M. Z.: Climate response of fossil fuel and biofuel soot, accounting for soot's feedback to snow and sea ice albedo and emissivity, J. Geophys. Res., 109, D21201, doi:10.1029/2004JD004945, 2004

Jaffe, D., Anderson, T., Covert, D., Kotchenruther, R., Trost, B., Danielson, J., Simpson, W., Blake, D., Harris, J. and Carmichael, G.: Transport of Asian Air Pollution to North America, , 26(6), 711–714, 1999.

Kaspari, S., Painter, T. H., Gysel, M., Skiles, S. M. and Schwikowski, M.: Seasonal and elevational variations of

639 black carbon and dust in snow and ice in the Solu-Khumbu, Nepal and estimated radiative forcings, Atmos.
640 Chem. Phys., 14(15), 8089–8103, doi:10.5194/acp-14-8089-2014, 2014.
641 Kaspari, S. D., Schwikowski, M., Gysel, M., Flanner, M. G., Kang, S., Hou, S. and Mayewski, P. A.: Recent
642 increase in black carbon concentrations from a Mt. Everest ice core spanning 1860-2000 AD, Geophys. Res.
643 Lett., 38(4), 11–16, doi:10.1029/2010GL046096, 2011.
644 Lamarque, J. and Hess, P. G.: Model analysis of the temporal and geographical origin of the CO distribution during
645 the TOPSE campaign, , 108, 1–12, doi:10.1029/2002JD002077, 2003.
646 Li, X., Kang, S., He, X., Qu, B., Tripathee, L., Jing, Z., Paudyal, R., Li, Y., Zhang, Y., Yan, F., Li, G. and Li, C.:
647 Light-absorbing impurities accelerate glacier melt in the Central Tibetan Plateau, Sci. Total Environ.,
648 doi:10.1016/j.scitotenv.2017.02.169, 2017.
649 Li, Y., Chen, J., Kang, S., Li, C., Qu, B., Tripathee, L., Yan, F., Zhang, Y., Guo, J., Gul, C. and Qin, X.: Impacts of
650 black carbon and mineral dust on radiative forcing and glacier melting during summer in the Qilian Mountains,
651 northeastern Tibetan Plateau, Cryosph. Discuss., (April), 1–14, doi:10.5194/tc-2016-32, 2016.
652 Lu, Z., Streets, D. G., Zhang, Q. and Wang, S.: A novel back-trajectory analysis of the origin of black carbon
653 transported to the Himalayas and Tibetan Plateau during 1996-2010, Geophys. Res. Lett., 39(1), 1–6,
654 doi:10.1029/2011GL049903, 2012.
655 Lüthi, Z. L., Škerlak, B., Kim, S. W., Lauer, A., Mues, A., Rupakheti, M. and Kang, S.: Atmospheric brown clouds
656 reach the Tibetan Plateau by crossing the Himalayas, Atmos. Chem. Phys., 15(11), 6007–6021, doi:10.5194/acp-
657 15-6007-2015, 2015.
658 Mahowald, N., Albani, S., Kok, J. F., Engelstaeder, S., Scanza, R., Ward, D. S. and Flanner, M. G.: The size
659 distribution of desert dust aerosols and its impact on the Earth system, Aeolian Res., 15, 53–71,
660 doi:10.1016/j.aeolia.2013.09.002, 2014.
661 Ménégoz, M., Krinner, G., Balkanski, Y., Cozic, a., Boucher, O. and Ciais, P.: Boreal and temperate snow cover
662 variations induced by black carbon emissions in the middle of the 21st century, Cryosph., 7, 537–554,
663 doi:10.5194/tc-7-537-2013, 2013.
664 Ménégoz, M., Krinner, G., Balkanski, Y., Boucher, O., Cozic, A., Lim, S., Ginot, P., Laj, P., Gallée, H., Wagnon, P.,
665 Marinoni, A. and Jacobi, H. W.: Snow cover sensitivity to black carbon deposition in the Himalayas: From
666 atmospheric and ice core measurements to regional climate simulations, Atmos. Chem. Phys., 14(8), 4237–4249,
667 doi:10.5194/acp-14-4237-2014, 2014.
668 Ming, J., Cachier, H., Xiao, C., Qin, D., Kang, S., Hou, S. and Xu, J.: Black carbon record based on a shallow
669 Himalayan ice core and its climatic implications, Atmos. Chem. Phy., 8, 1343–1352, doi:10.5194/acpd-7-14413-
670 2007, 2008.
671 Ming, J., Xiao, C., Cachier, H., Qin, D., Qin, X., Li, Z. and Pu, J.: Black Carbon (BC) in the snow of glaciers in west
672 China and its potential effects on albedos, Atmos. Res., 92(1), 114–123, doi:10.1016/j.atmosres.2008.09.007,
673 2009.

674 Ming, J., Xiao, C., Du, Z. and Yang, X.: An overview of black carbon deposition in High Asia glaciers and its
675 impacts on radiation balance, Adv. Water Resour., 55(May), 80–87, doi:10.1016/j.advwatres.2012.05.015, 2013a.
676 Ming, J., Du, Z., Xiao, C., Xu, X., and Zhang, D.: Darkening of the mid-Himalaya glaciers since 2000 and the
677 potential causes, Environ. Res. Lett., 7, 014021, doi:10.1088/1748-9326/7/1/014021, 2012.
678 Ming, J., Xiao, C., Wang, F., Li, Z. and Li, Y.: Grey Tienshan Urumqi Glacier No.1 and light-absorbing impurities,
679 Environ. Sci. Pollut. Res., 23(10), 9549–9558, doi:10.1007/s11356-016-6182-7, 2016.
680 Nair, V. S., Babu, S. S., Moorthy, K. K., Sharma, A. K., Marinoni, A. and Ajai: Black carbon aerosols over the
681 Himalayas: Direct and surface albedo forcing, Tellus, Ser. B Chem. Phys. Meteorol., 65(1),
682 doi:10.3402/tellusb.v65i0.19738, 2013.
683 Naoe, H., Hasegawa, S., Heintzenberg, J., Okada, K., Uchiyama, A., Zaizen, Y., Kobayashi, E., Yamazaki, A.: State
684 of mixture of atmospheric submicrometer black carbon particles and its effect on particulate light absorption,
685 Atmos. Environ., 43(6), 1296–1301, doi:org/10.1016/j.atmosenv.2008.11.031, 2009.
686 Niu, H., Kang, S., Shi, X., Paudyal, R., He, Y., Li, G. and Wang, S.: Science of the Total Environment In-situ
687 measurements of light-absorbing impurities in snow of glacier on Mt . Yulong and implications for radiative
688 forcing estimates, Sci. Total Environ., 581–582, 848–856, doi:10.1016/j.scitotenv.2017.01.032, 2017.
689 Painter, T. H., Deems, J. S., Belnap, J., Hamlet, A. F., Landry, C. C. and Udall, B.: Response of Colorado River
690 runoff to dust radiative forcing in snow., Proc. Natl. Acad. Sci. U. S. A., 107(40), 17125–30,
691 doi:10.1073/pnas.0913139107, 2010.
692 Pandolfi, M., Ripoll, A., Querol, X. and Alastuey, A.: Climatology of aerosol optical properties and black carbon
693 mass absorption cross section at a remote high-altitude site in the western Mediterranean Basin, Atmos. Chem.
694 Phys., 14(12), 6443–6460, doi:10.5194/acp-14-6443-2014, 2014.
695 Park, M., Randel, W. J., Emmons, L. K. and Livesey, N. J.: Transport pathways of carbon monoxide in the Asian
696 summer monsoon diagnosed from Model of Ozone and Related Tracers (MOZART), , 114, 1–11,
697 doi:10.1029/2008JD010621, 2009.
698 Qu, B., Ming, J., Kang, S. C., Zhang, G. S., Li, Y. W., Li, C. D., Zhao, S. Y., Ji, Z. M. and Cao, J. J.: The decreasing
699 albedo of the Zhadang glacier on western Nyainqentanglha and the role of light-absorbing impurities, Atmos.
700 Chem. Phys., 14(20), 11117–11128, doi:10.5194/acp-14-11117-2014, 2014.
701 Wang, J., He, X., Ye, B., and Yang, G.: Variations of Albedo on the Dongkemadi Glacier, Tanggula Range, Journal
702 of Glaciology and Geocryology, 34, 21–28, 2012.
703 Venkataraman, C., Habib, G., Eiguren-Fernandez, A., Miguel, A, H., Friedlander, S, K.:Residential Biofuels in
704 South Asia: Carbonaceous Aerosol Emissions and Climate Impacts, Science, 307 (5714), 1454-1456, doi:
705 10.1126/science.1104359, 2005.
706 Wang, M., Xu, B., Zhao, H., Cao, J., Joswiak, D., Wu, G. and Lin, S.: The Influence of Dust on Quantitative
707 Measurements of Black Carbon in Ice and Snow when Using a Thermal Optical Method, Aerosol Sci. Technol.,
708 46 (April 2017), 60–69, doi:10.1080/02786826.2011.605815, 2012.

709 Wang, Q., Jacob, D. J., Fisher, J. A., Mao, J., Leibensperger, E. M., Carouge, C. C., Le Sager, P., Kondo, Y.,
710 Jimenez, J. L., Cubison, M. J. and Doherty, S. J.: Sources of carbonaceous aerosols and deposited black carbon
711 in the Arctic in winter-spring: Implications for radiative forcing, Atmos. Chem. Phys., 11(23), 12453–12473,
712 doi:10.5194/acp-11-12453-2011, 2011.
713 Wang, X., Pu, W., Ren, Y., Zhang, X., Zhang, X., Shi, J., Jin, H., Dai, M. and Chen, Q.: Snow albedo reduction in
714 seasonal snow due to anthropogenic dust and carbonaceous aerosols across northern China, Atmos. Chem. Phys.
715 Discuss., (September), 1–52, doi:10.5194/acp-2016-667, 2016.
716 Warren, S. G.: Optical Properties of Snow (Paper 1R1505), Rev. Geophys. Sp. Phys., 20(1), 67 [online] Available
717 from: http://adsabs.harvard.edu/cgi-bin/nph-
718 data_query?bibcode=1982RvGSP..20...67W&link_type=EJOURNAL%5Cnpapers3://publication/doi/10.1029/R
719 G020i001p00067, 1982.
720 Warren, S. G. and Wiscombe, W. J.: Dirty snow after nuclear war, Nature, 313, 467–470, doi:10.1038/313467a0,
721 1985.
722 Xu, B., Cao, J., Hansen, J., Yao, T., Joswia, D. R., Wang, N., Wu, G., Wang, M., Zhao, H., Yang, W., Liu, X. and He,
723 J.: Black soot and the survival of Tibetan glaciers, Proc. Natl. Acad. Sci., 106(52), 22114–22118,
724 doi:10.1073/pnas.0910444106, 2009a.
725 Xu, B., Cao, J., Joswiak, D. R., Liu, X., Zhao, H. and He, J.: Post-depositional enrichment of black soot in snow-
726 pack and accelerated melting of Tibetan glaciers, Environ. Res. Lett., 7(1), 14022, doi:10.1088/1748-
727 9326/7/1/014022, 2012.
728 Yang, S., Xu, B., Cao, J., Zender, C. S. and Wang, M.: Climate effect of black carbon aerosol in a Tibetan Plateau
729 glacier, Atmos. Environ., 111, 71–78, doi:10.1016/j.atmosenv.2015.03.016, 2015.
730 Yasunari, T. J., Bonasoni, P., Laj, P., Fujita, K., Vuillermoz, E., Marinoni, A., Cristofanelli, P., Duchi, R., Tartari, G.
731 and Lau, K. M.: Estimated impact of black carbon deposition during pre-monsoon season from Nepal Climate
732 Observatory - Pyramid data and snow albedo changes over Himalayan glaciers, Atmos. Chem. Phys., 10(14),
733 6603–6615, doi:10.5194/acp-10-6603-2010, 2010.
734 Yasunari, T. J., Lau, K.-M., Mahanama, S. P. P., Colarco, P. R., Silva, A. M. Da, Aoki, T., Aoki, K., Murao, N.,
735 Yamagata, S. and Kodama, Y.: The GOddard SnoW Impurity Module (GOSWIM) for the NASA GEOS-5 Earth
736 System Model: Preliminary Comparisons with Observations in Sapporo, Japan, Sola, 10(MAY), 50–56,
737 doi:10.2151/sola.2014-011, 2014.
738 Zhang, G., Kang, S., Fujita, K., Huintjes, E., Xu, J., Yamazaki, T., Haginoya, S., Wei, Y., Scherer, D., Schneider, C.
739 and Yao, T.: Energy and mass balance of Zhadang glacier surface, central Tibetan Plateau, J. Glaciol., 59(213),
740 137–148, doi:10.3189/2013JoG12J152, 2013.
741 Zhang, Y., Kang, S., Xu, M., Sprenger, M., Gao, T., Cong, Z., Li, C., Guo, J., Xu, Z., Li, Y., Li, G., Li, X., Liu, Y.
742 and Han, H.: Sciences in Cold and Arid Regions Light-absorbing impurities on Keqikaer Glacier in western Tien
743 Shan : concentrations and potential impact on albedo reduction, , 9(2), doi:10.3724/SP.J.1226.2017.00097.Light-

absorbing, 2017.

Zhang, Y., Hirabayashi, Y., Liu, Q. and Liu, S.: Glacier runoff and its impact in a highly glacierized catchment in the southeastern Tibetan Plateau: Past and future trends, J. Glaciol., 61(228), 713–730, doi:10.3189/2015JoG14J188, 2015.

Atmos. Chem. Phys. Discuss., https://doi.org/10.5194/acp-2017-667
Manuscript under review for journal Atmos. Chem. Phys.
Discussion started: 28 August 2017

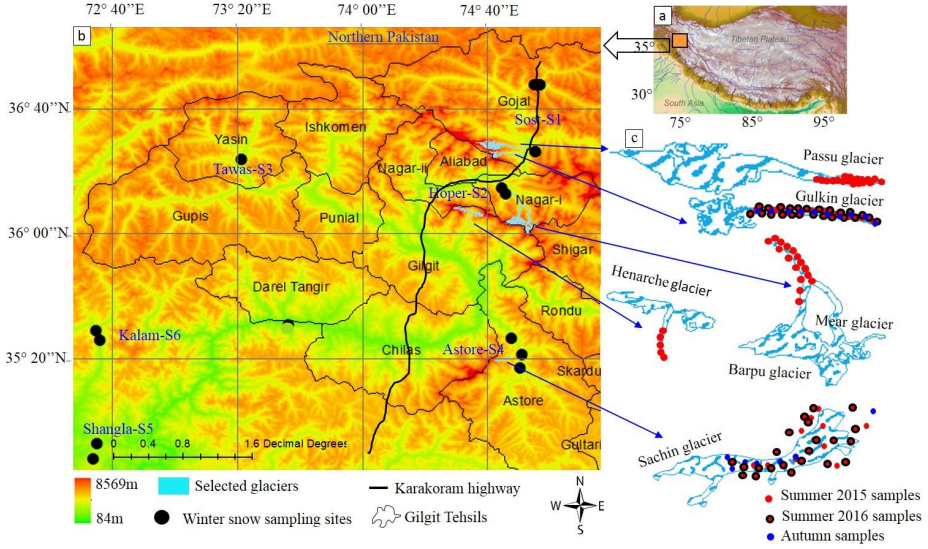

Figure 1. The study area and sampling sites: (a) Himalayan mountain range and Tibetan Plateau, (b) winter sampling sites (solid black circles), (c) glaciers selected for summer and autumn sampling

Atmos. Chem. Phys. Discuss., https://doi.org/10.5194/acp-2017-667
Manuscript under review for journal Atmos. Chem. Phys.
Discussion started: 28 August 2017

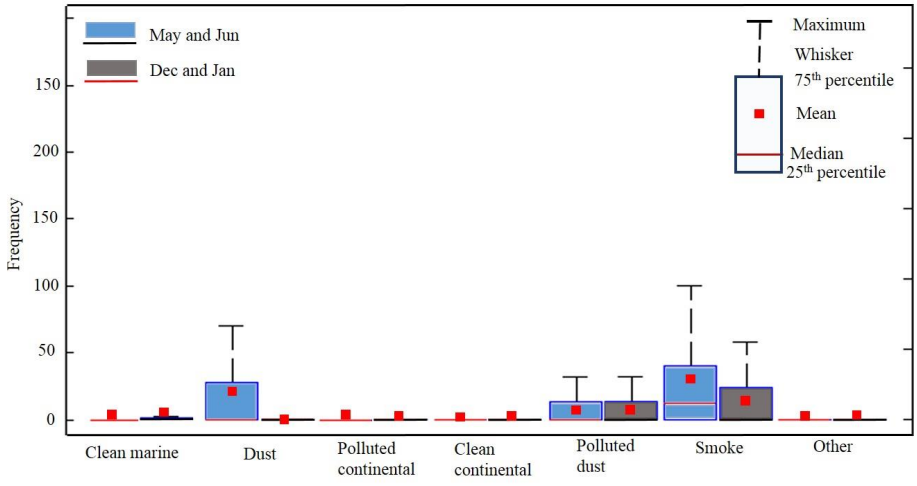

754

755 **Figure 2. Frequency distribution of aerosol subtypes in the atmosphere over the study region calculated from CALIPSO data for the months in 2006 to 2014**

Atmos. Chem. Phys. Discuss., https://doi.org/10.5194/acp-2017-667
Manuscript under review for journal Atmos. Chem. Phys.
Discussion started: 28 August 2017

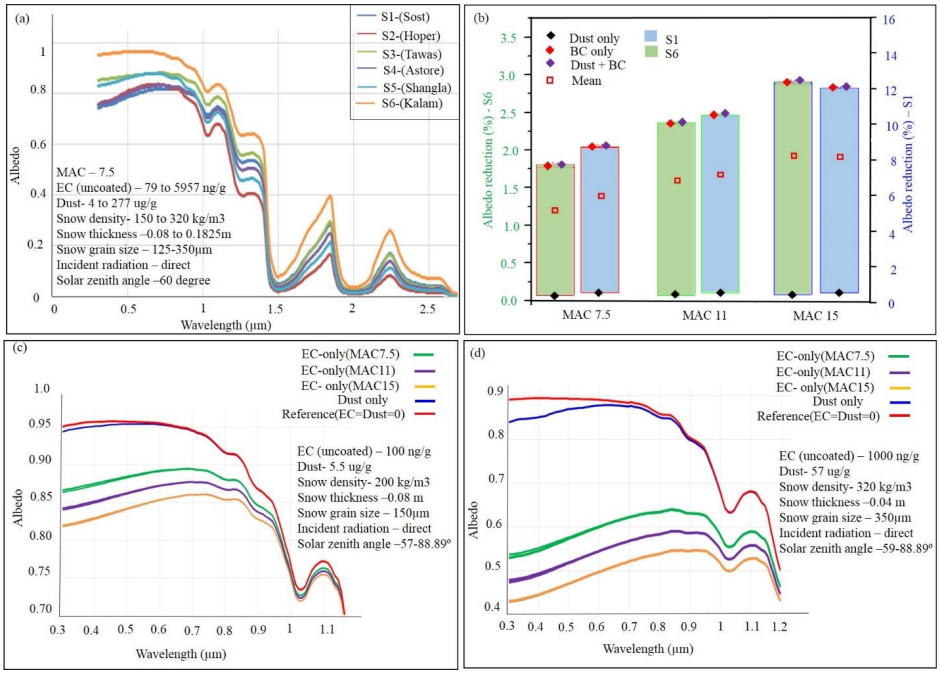

Figure 3. Spectral variation in albedo for winter sampling sites and selected MAC values, (a) average albedo of samples at each of the sites (b) daily mean albedo reduction of fresh snow (site S6) and aged snow (site S1) snow, (note different scales of y axis) (c) albedo of fresh snow site S6, (d) albedo of aged snow site S1.

Atmos. Chem. Phys. Discuss., https://doi.org/10.5194/acp-2017-667
Manuscript under review for journal Atmos. Chem. Phys.
Discussion started: 28 August 2017

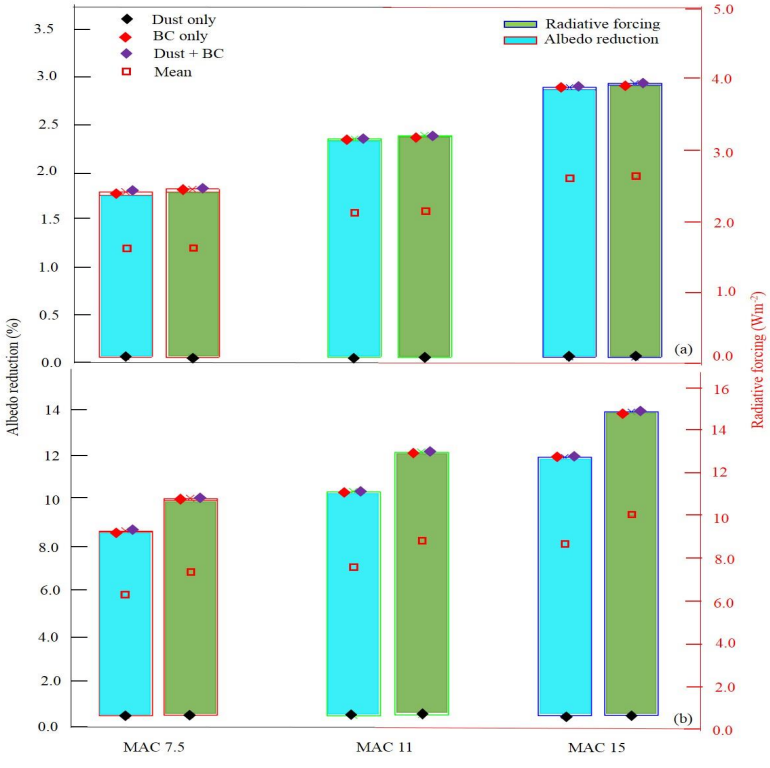

Figure 4. Daily mean radiative forcing (%) and albedo reduction (%) caused by BC and dust in (a) fresh (low BC) and (b) aged (high BC) snow samples (note different scales of y axis)

Atmos. Chem. Phys. Discuss., https://doi.org/10.5194/acp-2017-667
Manuscript under review for journal Atmos. Chem. Phys.
Discussion started: 28 August 2017

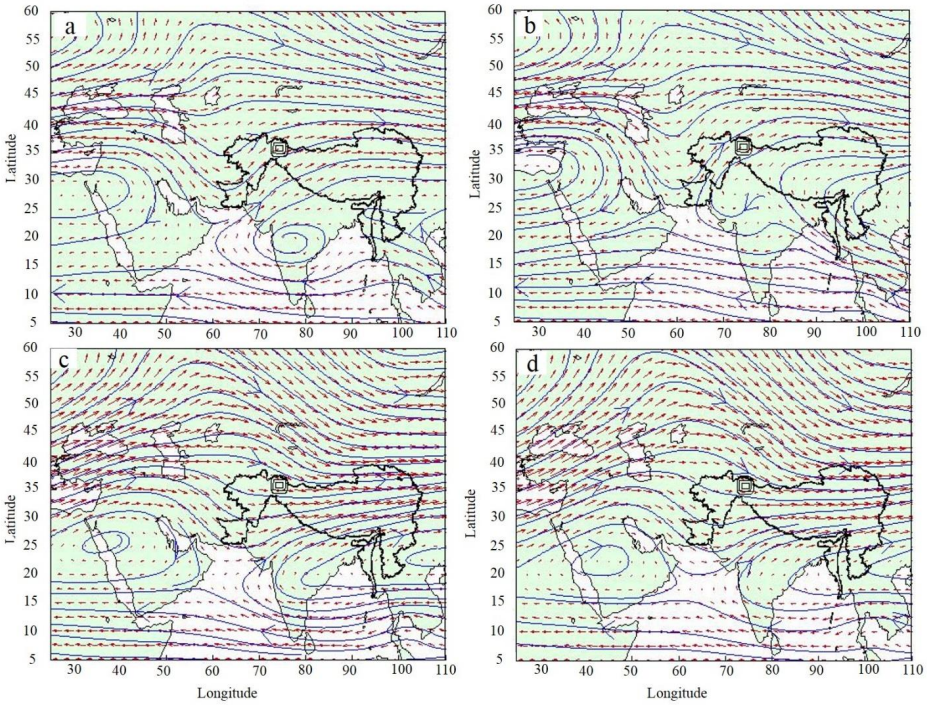

Figure 5. Fifty years monthly average horizontal wind patterns at 700 hPa during a) May, b) June, c) December, and d) January, corresponding to approximately 3000 masl, from NCEP NCAR. The study area is indicated by a square.

Atmos. Chem. Phys. Discuss., https://doi.org/10.5194/acp-2017-667
Manuscript under review for journal Atmos. Chem. Phys.
Discussion started: 28 August 2017

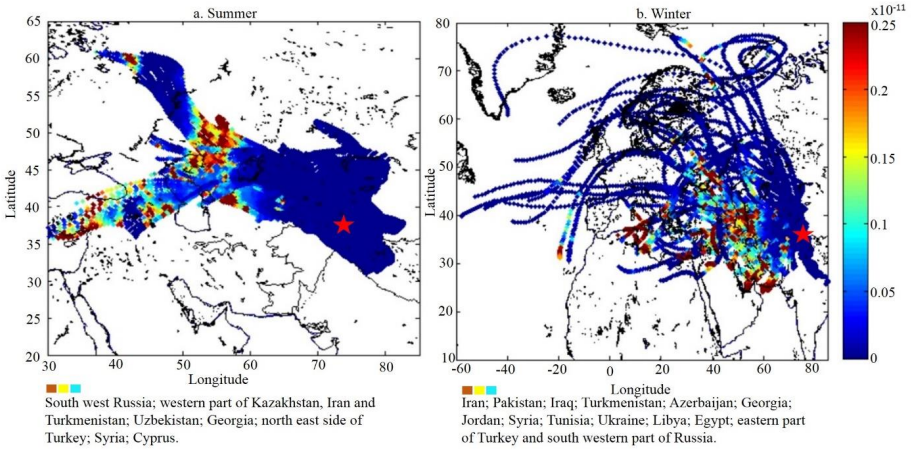

Figure 6. Source contribution regions of pollutants identified using an emissions inventory coupled with back trajectories. Red star indicates the position of the study area.

Atmos. Chem. Phys. Discuss., https://doi.org/10.5194/acp-2017-667
Manuscript under review for journal Atmos. Chem. Phys.
Discussion started: 28 August 2017

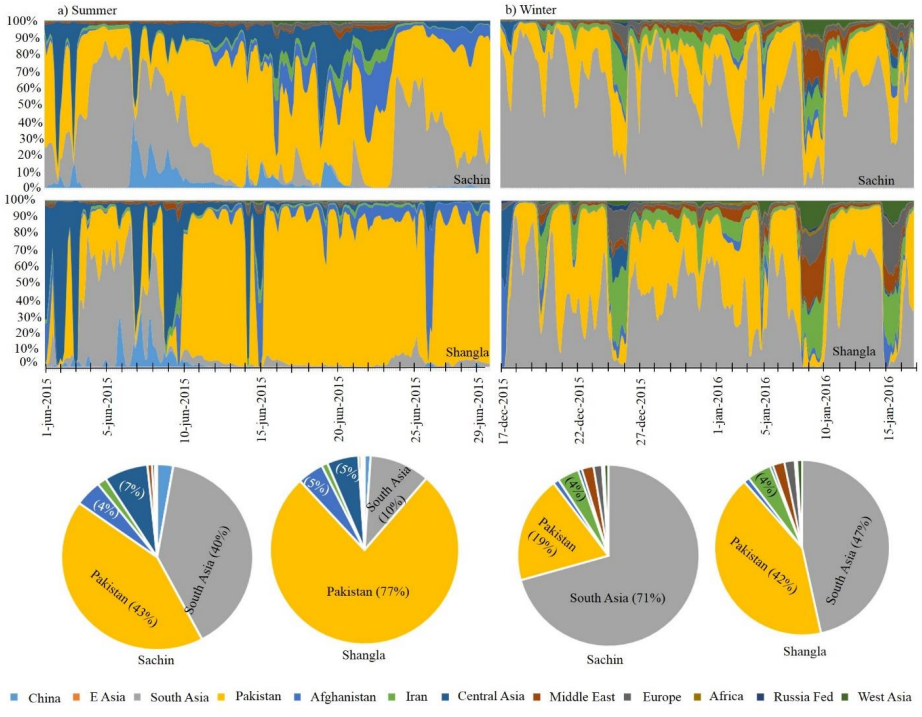

Figure 7. Source contribution regions of carbon monoxide for selected sites identified by WRF-STEM during (a) summer and (b) winter seasons.

Atmos. Chem. Phys. Discuss., https://doi.org/10.5194/acp-2017-667
Manuscript under review for journal Atmos. Chem. Phys.
Discussion started: 28 August 2017

Atmospheric Chemistry and Physics Discussions

775 **Table 1. Concentration of BC, OC, and dust in summer, autumn, and winter samples in 2015 and 2016.**

Glacier/ Site	No.	Elevation (masl) min–max	BC min–max (avg) (ngg^{-1})	OC min–max (avg) (ngg^{-1})	Dust min–max (avg) (μgg^{-1})	Type[a] / snow age in days	OC/BC[b]	Year
Summer (May 2015/ May 2016)								
Barpu	6	2901–3405	877–5994 (2938)	244–1228 (691)	292–5250 (1998)	DCI	0.07–1.38	2015
Gulkin	31	2741–3319	82–5676 (1327)	238–8514 (1594)	31–2039 (648)	DCIS	0.169–3.76	2015/16
Henarche	4	2569–2989	778–10502 (4820)	275–4176 (1628)	225–2723 (993)	Ice	0.04–1.63	2015
Mear	8	2961–3539	222–3656 (1593)	703–6588 (2992)	33–656 (211)	DCI	0.72–4.88	2015
Passu	14	2663–3158	87–734 (346)	132–1810 (741)	28–524 (196)	DCI	1.85–4.80	2015
Sachin	35	3414–3895	257–4127 (1769)	128–7592 (3348)	5.6–2495 (314)	DCIS	0.08–0.53	2015/16
Total	98							
Autumn (October 2016)								
Gulkin	7	2741–3319	125–1028 (451)	266–3574 (1276)	60–767 (253)	DCIS	1.29–3.59	2016
Sachin	6	3414–3895	4342–6481 (5314)	543–3478 (1571)	124–1348 (546)	DCIS	0.11–0.53	2016
Total	13							
Winter (Dec 2015/ Jan 2016)								
S1-Sost	6	2873–3092	482–5957 (2506)	378–2934 (1039)	29–311 (131)	2–17 d	0.25–0.78	2015
S2-Hopar	2	2602–2794	229–1064 (646)	330–1976 (1153)	23–129 (76)	1–15 d	1.4–1.8	2016
S3-Tawas	1	2437	650	1320	16	8–17 d	2.03	2016
S4-Astore	3	2132–2396	450–2640 (1305)	914–3645 (2161)	55–171 (97)	4–7 d	1.38–2.33	2016
S5-Shangla	2	2324–2373	367–1110 (739)	1302–2856 (2079)	13–49 (31)	8–9 d	2.5–3.5	2016
S6-Kalam	4	1933–2101	79–123 (107)	214–558 (347)	4–6 (5)	1 d	2.3–5	2016
Total	18							

776 [a] type = snow or ice type; DCI = debris-covered ice; DCIS = debris-covered ice and aged snow

777 [b] range of OC/BC in individual samples

Atmos. Chem. Phys. Discuss., https://doi.org/10.5194/acp-2017-667
Manuscript under review for journal Atmos. Chem. Phys.
Discussion started: 28 August 2017

Atmospheric Chemistry and Physics Discussions

778

779 **Table 2. Snow albedo reduction (%) at 0.975 μm by BC, dust, and BC plus dust at the site with the lowest average pollutant concentration (S6) and the site with the highest**
780 **average pollutant concentration (S1), under different MAC values.**

Pollutant	MAC	Low concentration site (S6)			High concentration site (S1)		
	(m^2/g)	Daytime min	Daytime max	Daily mean	Daytime min	Daytime max	Daily mean
BC	7.5	2.8	5.1	1.8	15.6	23.9	9.0
	11	3.7	6.9	2.3	19.2	28.6	10.5
	15	4.6	8.3	2.9	22.3	32.5	12.0
Dust	7.5	0.1	0.2	0.07	0.9	1.6	0.05
	11	0.1	0.2	0.07	0.9	1.6	0.05
	15	0.1	0.2	0.07	0.9	1.6	0.05
BC and dust	7.5	2.9	5.2	1.8	15.7	24.0	8.8
	11	3.8	6.8	2.4	19.2	28.6	10.5
	15	4.6	8.3	2.9	22.3	32.5	12.0

781